Free-space nitrogen gas laser driven by a femtosecond filament

Daniil Kartashov,[1,*] Skirmantas Ališauskas,[1] Giedrius Andriukaitis,[1] Audrius Pugžlys,[1] Mikhail Shneider,[2] Aleksei Zheltikov,[3,4] See Leang Chin,[5] and Andrius Baltuška[1]

[1]*Photonics Institute, Vienna University of Technology, Gusshausstrasse 27-387, A 1040, Vienna, Austria*

[2]*Department of Mechanical and Aerospace Engineering, Princeton University, Princeton, New Jersey 08544-5263, USA*

[3]*Physics Department, Russian Quantum Center, International Laser Center, M.V. Lomonosov Moscow State University, 119992 Moscow, Russia*

[4]*Department of Physics and Astronomy, Texas A&M University, College Station, Texas, 77843-4242, USA*

[5]*Center for Optics, Photonics and Laser (COPL), Laval University, Quebec, Qc GIK 7P4, Canada*

(Received 17 November 2011; published 24 September 2012)

We report an experimental proof and full characterization of laser generation in molecular nitrogen in an argon-nitrogen gas mixture remotely excited at a distance above 2 m in a femtosecond laser filament. Filamentation experiments performed with near-infrared, 1-μm-wavelength and midinfrared, 4-μm-wavelength short-pulse laser sources show that mid-IR laser pulses enable radical enhancement of filamentation-assisted lasing by N_2 molecules. Energies as high as 3.5 μJ are achieved for the 337- and 357-nm laser pulses generated through the second-positive-band transitions of N_2, corresponding to a 0.5% total conversion efficiency from midinfrared laser energy to the energy of UV lasing.

DOI: 10.1103/PhysRevA.86.033831 PACS number(s): 42.55.Lt, 42.65.Jx, 42.72.Bj, 82.33.Xj

I. INTRODUCTION

Lasing from molecular nitrogen was observed for the first time in the early 1960s, at the dawn of the laser era [1,2]. Today the discharge-pumped nitrogen laser, operating in a broad range of gas pressures, from several millibars to the atmospheric pressure, and repetition rates from several hertz to several kilohertz, is a cheap and robust source of high-power near-UV radiation. Because of the abundance of nitrogen in Earth's atmosphere, achieving nitrogen lasing via remote excitation would pave the way to many potential applications. In particular, such a narrowband source of stimulated emission would provide coherent, highly directional radiation for highly selective and sensitive remote spectroscopy of the atmosphere [3,4]. The possibility for remote ignition of a free-localized nitrogen laser in air was demonstrated previously in a microwave discharge [5]. In Ref. [5] it was also suggested that it might be possible to excite free-space nitrogen lasing by focused laser beams.

The discovery of the process of femtosecond filamentation in gases [6] has retriggered the quest for a remotely excited free-space nitrogen laser. Filamentation of high-power femtosecond laser radiation in gases manifests itself in the formation of a self-guided, high-intensity field structure, accompanied by a significant spectral broadening, supercontinuum generation, and creation of a plasma channel in the wake of the pulse. Femtosecond filaments can be generated at standoff distances of up to tens of kilometers and form ionized channels of up to hundreds of meters [7–12]. Formation of plasma in the filament, similar to a gas discharge [13], initiates a chain of plasma-chemical reactions in the atmosphere which lead to the appearance of a large variety of neutral and ionic species in rotationally, vibrationally, and electronically excited states. As one of the consequences, favorable conditions for population inversion and lasing between different electronic levels in nitrogen and in oxygen might be created [14]. Note that standoff lasing of oxygen in the atmosphere, initiated by the resonant multiphoton excitation with the UV nanosecond laser, was demonstrated recently [15]. Realization of standoff lasing with a femtosecond filament will have an obvious advantage in comparison to this scheme due to substantially less scattering and absorption losses.

The possibility of stimulated emission from nitrogen in femtosecond filaments was discussed for the first time in Ref. [16]. The only proof of lasing was based on the exponential fit of the dependence of fluorescence on the filament length. First, it is worth noticing that such exponential dependence would be valid under the condition of a stationary population inversion only. This is obviously not the case in the filament-driven laser because "the pump" is the femtosecond laser pulse and amplified spontaneous emission (ASE) develops about a nanosecond later. Thus, laser generation would build up under the condition of a decaying population inversion which has a decay rate on the same nanosecond time scale. Second, the filament length was calculated from the laser power assuming the direct proportionality between these values. However, the experiment in Ref. [16] was carried out with the laser power ranging from about 11 to 170 critical powers of self-focusing, assuming the value of the critical power in air to be 3 GW [12]. Multiple filament formation is expected at such high levels of laser power, and the assumption that the filament length is simply proportional to the laser power, used in Ref. [16], is not valid.

In this article, we report on a successful generation of microjoule pulses from a cavity-free nitrogen laser that uses the plasma channel traced by a femtosecond laser filament as its active medium. In this lasing process, the electronic transitions of nitrogen are the same as in the conventional discharge-pumped nitrogen laser [17]. However, the physics behind the population inversion in our situation is substantially different. In the discharge-driven scheme, the upper lasing triplet state $C\ ^3\Pi_u$ in the three-level nitrogen laser is populated

*daniil.kartashov@tuwien.ac.at

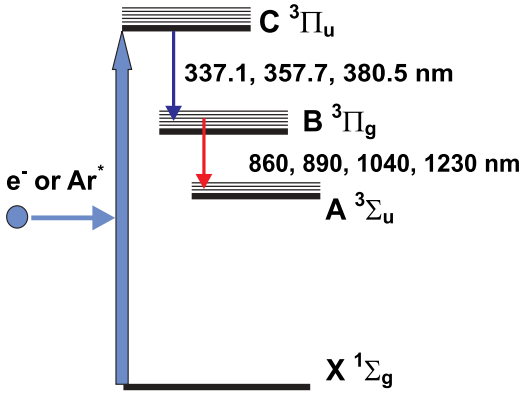

FIG. 1. (Color online) Energy-level diagram of a collisionally pumped nitrogen laser.

by electron impact excitation from the singlet ground state $X\,^1\Sigma_g$, as shown in Fig. 1. This gives rise to an efficient fluorescence in the near-UV (300–400 nm) spectral range due to radiative transitions between the vibrational manifolds of the $C\,^3\Pi_u$ and $B\,^3\Pi_g$ states. Control over the density and temperature of electrons is of key importance for obtaining population inversion and lasing between these states. Under the conditions of impulsive rf or capacitor discharge, rapid Joule heating of electrons due to collisions with neutrals leads to the formation of a nonequilibrium energy distribution of electrons [13]. The nonequilibrium energy distribution and the plasma concentration are maintained throughout the discharge, resulting in a sufficient amount of hot electrons with kinetic energies around 15 eV—the peak of the excitation cross section for the $C\,^3\Pi_u$ state [18]—which is needed for efficient pumping.

By contrast, in a laser filament, the electronic energy distribution is formed on the time scale of the femtosecond laser pulse by the optical field ionization process. After the femtosecond pulse, the resultant energy distribution function evolves freely as the plasma concentration decays. Therefore, the required $C\,^3\Pi_u$ excitation by electron impact can only be achieved within about 1 ns, i.e., the average lifetime of the plasma electrons. Thus, using a single femtosecond pulse, it is not possible to control the electron temperature during the buildup of population inversion, nor to control the duration of the time window within which the nitrogen laser is pumped. By contrast to the electric discharge pumping, which maintains hot plasma, in the femtosecond filament the optimal electronic energy distribution is governed by optical field ionization and therefore is determined by the intensity and the optical cycle duration. Unfortunately, the effect of intensity clamping [19,20] precludes the possibility of direct scaling of the temperature of electrons in a filament via an increase of the pulse energy. Also, the plasma density is limited by the self-consistent balance between self-focusing and plasma refraction when focusing conditions are fixed [19,20]. Additionally, intensity clamping sets the filament diameter, which for 0.8-μm laser pulses is about 100 μm [7–12]. The coherence length of ASE is chiefly determined by the radiative lifetime (~1 ns at the atmospheric pressure) and, therefore, is ~30 cm. Correspondingly, the minimum gain required to overcome diffraction losses should amount to ~0.3 cm^{-1}.

In this paper we experimentally demonstrate efficient lasing of molecular nitrogen in a femtosecond filament. To find a way around the problem of control over the electronic temperature, we exploit the process of resonant excitation transfer from excited noble gas atoms to molecules [21] in a nitrogen-argon mixture. Excited metastable atoms of argon are produced as a result of a two-step kinetic process in the filament plasma involving three-body collisions $Ar^+ + 2Ar \rightarrow Ar_2^+ + Ar$ and dissociative recombination $Ar_2^+ + e \rightarrow Ar^*(4\,^3P_2) + Ar$. Population inversion in nitrogen is achieved due to $Ar^*(4\,^3P_2) + N_2(X\,^1\Sigma_g) \rightarrow Ar + N_2(C\,^3\Pi_u)$ collisions (Fig. 1). This process transfers the excitation energy of argon atoms to molecular nitrogen. Thus, excited argon atoms can provide a collisional pump for laser transitions of N_2 in a laser-induced filament, playing the same role as the one played by hot electrons in a discharge-pumped nitrogen laser.

II. EXPERIMENTAL RESULTS

In our filament-assisted nitrogen lasing experiments, we used a novel high-power midinfrared (mid-IR) optical parametric source, providing 80-fs, 8-mJ pulses at a 20-Hz repetition rate at a wavelength of 3.9 μm [22]. The beam was focused by a $f = 2$ m focusing lens into a 4-m-long gas cell with Brewster-angled input and output windows made of CaF_2. An uncoated CaF_2 plate was inserted into the input beam to enable characterization of backward emission from

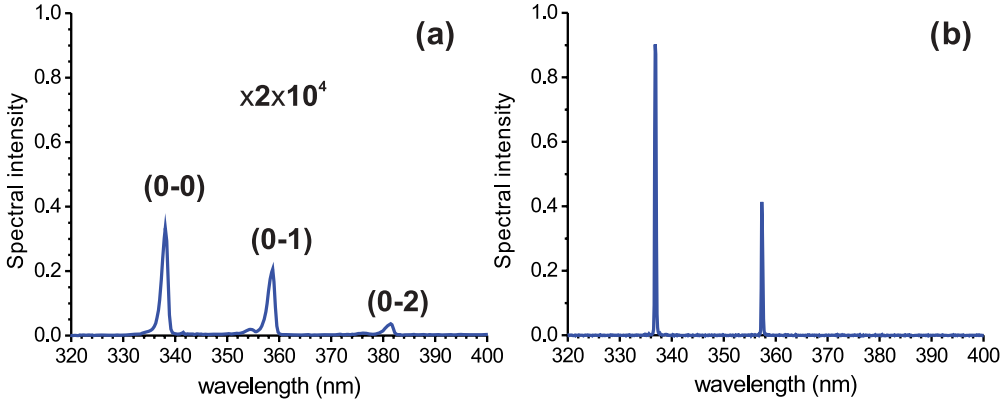

FIG. 2. (Color online) Spectra of (a) fluorescence from 1 bar of pure nitrogen and (b) lasing from the 1 bar of N_2 and 5 bars of Ar mixture. Vibrational levels for C-B electronic transition are assigned.

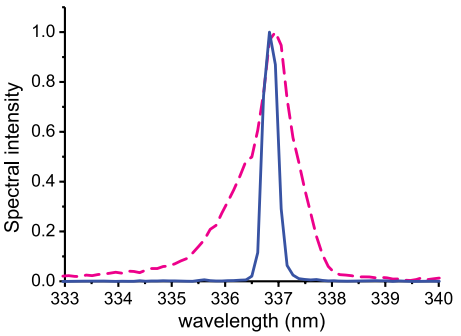

FIG. 3. (Color online) Spectrum of backward fluorescence (dashed line, violet curve) and backward-directed ASE (solid line, blue curve).

the filament. A fast photodiode, a spectrometer, and a CCD camera were used, respectively, for the temporal, spectral, and spatial characterization of nitrogen fluorescence and lasing. Formation of a filament in the cell was confirmed by a strong shift of the focal position in the direction of the laser source and appearance of a low-divergence self-guided beam structure at the cell output accompanied by the conical emission of a supercontinuum [23].

The results of the measurement are summarized in Fig. 2. Below the lasing threshold, a well-known UV fluorescence spectrum of N_2 was observed from the gas cell [Fig. 2(a)]. At the input mid-IR pulse energy of 7 mJ, backward UV nitrogen lasing from the gas cell was observed at the nitrogen pressure above 0.3 bar and the argon pressure above 3 bar. Stimulated emission from nitrogen in the forward direction was not studied due to the background of the broadband supercontinuum emission. Lasing was achieved simultaneously for two lines at 337 and 357 nm, belonging to the second positive band of N_2. These lines correspond, respectively, to the transitions from the lowest vibrational level of the upper $C\,^3\Pi_u$ state to the lowest and first excited vibrational levels of the $B\,^3\Pi_g$ electronic state [Fig. 2(b)]. Measurements with a high-resolution spectrometer confirm substantial spectrum narrowing of the UV lines when laser generation is achieved, as it is shown in Fig. 3 for the 337-nm emission line.

We have investigated the threshold and efficiency of lasing as a function of partial pressures of nitrogen and argon in the gas mixture. The results are summarized in Fig. 4. At a fixed nitrogen pressure, the lasing efficiency increases with the increase of argon pressure and saturates at around 6 bar [Fig. 4(a)]. At a fixed argon pressure, first the lasing efficiency increases with the increase of nitrogen pressure and then drops after passing a broad maximum at around 1.7 bar [Fig. 4(b)]. This drop of efficiency at high nitrogen pressures can be explained by the collisional quenching of the population inversion: $N_2(C\,^3\Pi_u) + N_2(X\,^1\Sigma_g) \rightarrow N_4 \rightarrow N_2(B\,^3\Pi_g$ vibr. excited$) + N_2(X\,^1\Sigma_g)$.

For the optimal mixture (1 bar N_2 and 5 bar Ar), the measured sum energy at 337 and 357 nm lines reached up to 3.5 μJ, corresponding to a 0.5% energy conversion efficiency from the midinfrared laser pulse to UV radiation. For comparison, in a discharge-pumped laser, typically less than 0.1% of the electric energy in the discharge is converted into the laser emission.

The temporal profiles of the N_2 laser pulses at 337 and 357 nm are presented in Fig. 5(a) after deconvolution with the response function of the fast photodiode used in the measurement. Interference filters with peak transmission at 340 and 360 nm and FWHM of 10 nm were used to acquire individual temporal profiles at the two emission lines. As evidenced by Fig. 5(a), lasing at 337 nm develops about a nanosecond earlier than at 357 nm and is emitted as a shorter subnanosecond pulse, whereas the duration of a 357-nm pulse is about 2 ns FWHM. The measured spatial beam profile is shown in Fig. 5(b) and has a roughly super-Gaussian shape. Low beam divergence of about 1.6 mrad was retrieved by measuring the beam profile as a function of the distance from the gas cell. Insertion of a 2-mm-thick CaF_2 parallel plate in the beam results in the appearance of clearly seen interference fringes [see inset on Fig. 5(b)], proving a high temporal coherency of the generated UV emission.

Under real atmospheric conditions, the presence of oxygen will strongly influence the lasing. It was shown that collisions with oxygen molecules led to very efficient quenching of the excited electronic states of molecular nitrogen [24]: $N_2(C\,^3\Pi_u) + O_2(X\,^3\Sigma_g) \rightarrow O + O + N_2(X\,^1\Sigma_g)$. This process has a very high rate constant $\sim 3 \times 10^{-10}$ cm^3 s^{-1} [24], which is more than an order of magnitude higher than the rate constants of quenching in nitrogen-nitrogen collisions and other parasitic reactions, like dissociative recombination, three-body

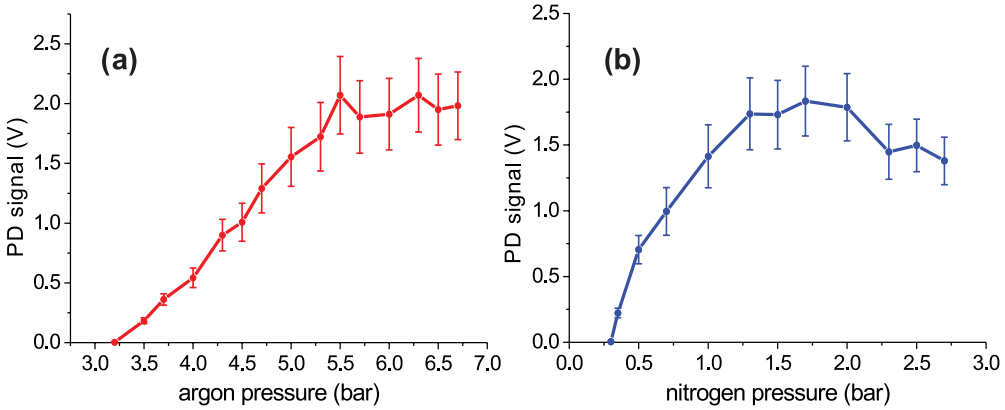

FIG. 4. (Color online) Dependence of the total lasing efficiency on (a) partial pressure of argon for fixed partial pressure of nitrogen 1 bar, and (b) partial pressure of nitrogen for fixed partial pressure of argon 5 bar.

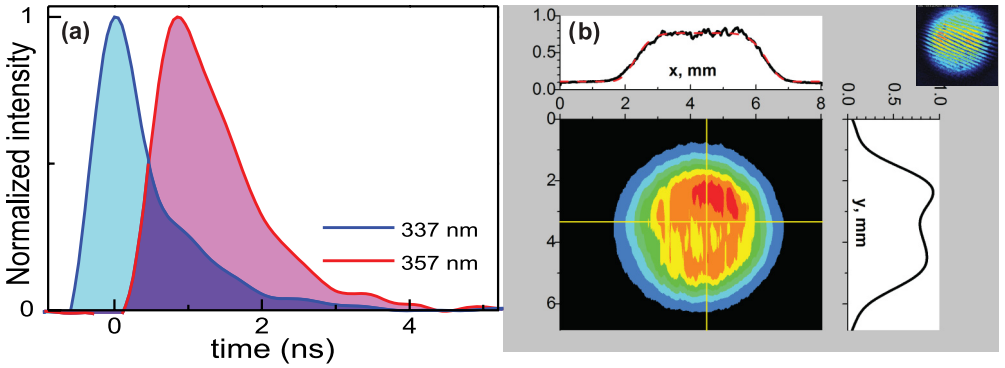

FIG. 5. (Color online) (a) Temporal profiles of the 337-nm (blue solid curve) and 357-nm (magenta dashed curve) laser pulses from the nitrogen-argon mixture. (b) The UV-lasing beam profile. The red dotted line shows a 6th-power super-Gaussian fit. Insert is a CCD image of interference in the beam from a 2-mm-thick CaF_2 parallel plate.

recombination, and attachment, which would effectively reduce lasing efficiency [25]. To investigate the influence of oxygen, we measured the UV lasing yield as a function of oxygen pressure by adding air to the nitrogen-argon mixture under a constant total pressure of 1 bar nitrogen. The results of the measurements are presented in Fig. 6. These experiments reveal an exponential decrease of the lasing power as a function of the O_2 pressure with a complete suppression of lasing in a mixture where the oxygen content is above 5%.

To investigate the influence of the ionizing pulse wavelength on the robustness of the nitrogen lasing from a filament, we repeated the experiments using a near-infrared filament created by 200–fs, $\leqslant$6–mJ, 1.03–μm pulses from a 0.5–kHz repetition rateYb:CaF_2 laser. With the 1.03–μm driving source nitrogen lasing in an N_2-Ar mixture was also achieved and the optimal partial gas pressures were nearly identical to the case of mid-IR excitation, although the threshold pressures of nitrogen and argon where higher. However, the lasing was only obtained at the stronger 337-nm line with a substantially lower efficiency. The wavelength dependence of free-space lasing characteristics initiated by filaments needs further detailed investigation. Here, we would like to point out the crucial role of the wavelength scaling law in femtosecond filamentation. Because of the λ^2 dependence of the critical power of self-focusing, for the conditions of N_2 lasing, a single filament was possible with mid-IR excitation, as opposed to a distinctly multiple-filament regime with 1-μm excitation. We assume that splitting of one long plasma channel into several shorter channels under the multiple-filamentation conditions might reduce ASE gain substantially and, therefore, terminate the lasing. Also, our numerical simulations of the mid-IR filamentation show that a larger diameter plasma channel with the higher plasma density than in the near-IR filament can be formed under our experimental conditions (see the next section). This leads to the reduction of the diffraction losses and decrease in the threshold gas pressure necessary to achieve lasing, as it is observed in the experiment, and increase in total generated power.

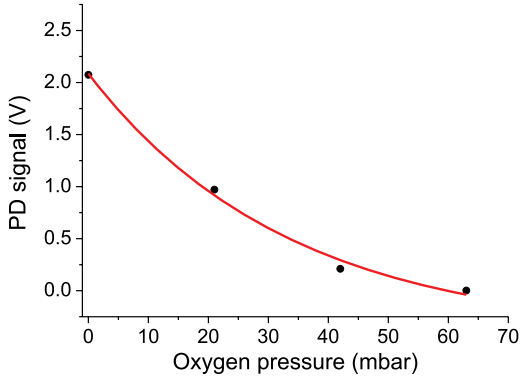

FIG. 6. (Color online) Experimentally measured lasing efficiency as a function of partial oxygen pressure (dots) in the argon-nitrogen mixture for 1 bar of the partial nitrogen pressure and 5 bars of the partial argon pressure. The solid line shows exponential fit.

III. NUMERICAL MODELING

The model used to analyze the lasing in a laser-induced filament includes the descriptions of filamentation dynamics and of plasma kinetics in the wake of the filament. The electron density and the intensity of the laser pulses, retrieved from these calculations, were then used to solve the system of plasma kinetics equations jointly with the equations for the electron temperature and the vibrational temperature of ground-state nitrogen molecules. To include the lasing effects, the set of plasma kinetic equations is completed by the relevant rate equations for the populations of the lasing levels and number of emitted photons.

A. Filamentation modeling

Filamentation is modeled by numerically solving the cylindrically symmetric nonlinear Schrödinger equation, which accounts for the impact of plasma dispersion and refraction, beam diffraction, as well as Kerr, Raman, and plasma nonlinearities [7,8,26]:

$$\frac{\partial}{\partial z}A(\omega,r,z) = \left[\frac{ic}{2\omega}\Delta_\perp + i\hat{D}(\omega) - \omega\kappa(\omega)/c\right]A(\omega,r,z) + \hat{F}\left\{i\frac{\omega_0}{c}\hat{T}[\delta(\eta)n_2(1-f_R)|A(\eta,r,z)|^2 + n_2 f_R\int_{-\infty}^{\infty}R(\eta-\eta')I(\eta',r,z)d\eta'\right.$$

$$+\frac{n_2(1-f_R)}{3}e^{-2i\omega_0 t}A^2(\eta,r,z)$$
$$+n_4|A(\eta,r,z)|^4]A(\eta,r,z)$$
$$-\left(i\frac{\omega_0}{2cn_0^2\rho_c}\hat{T}\rho+\frac{U_i W(\rho_0-\rho)}{2I}+\frac{\sigma}{2}\rho\right)$$
$$\times A(\eta,r,z)\Bigg\}. \quad (1)$$

Here, $A(\eta,r,z)$ is the complex field amplitude, $A(\omega,r,z)$ is its Fourier transform, $I=|A(\eta,r,z)|^2$ is the field intensity, z is the coordinate along the propagation path, r is the radial coordinate, $\eta=t-z/u$ is the time in the retarded frame of reference, t is the time in the laboratory frame of reference, u is the group velocity, r is the radial coordinate, $\omega=2\pi c/\lambda$ is the frequency of the field with the wavelength λ, $\Delta_\perp=r^{-1}\partial(r\partial/\partial r)/\partial r$ is the diffraction operator, $\hat{D}=k(\omega)-k(\omega_0)-\partial k/\partial\omega|_{\omega_0}(\omega-\omega_0)$ is the dispersion operator, ω_0 is the central frequency of the input laser field, $k(\omega)=\omega n(\omega)/c$, $n(\omega)-i\kappa(\omega)$ is the complex refractive index of the gas, $n_0=n(\omega_0)$, $\hat{F}$ is the Fourier transform operator, n_2 and n_4 are the nonlinear refractive index coefficients, c is the speed of light in vacuum, $\hat{T}=1+i\omega_0^{-1}\partial/\partial\eta$, $R(\eta)$ is the Raman function of the gas, ρ is the electron density, ρ_0 is the initial density of neutral atoms, U_i is the ionization potential, W is the ionization rate, σ is the impact ionization cross section, $\rho_c=\omega_0^2 m_e\varepsilon_0/e^2$ is the critical plasma density, m_e and e are the electron mass and charge, and ε_0 is vacuum permittivity.

The pulse propagation equation (1) is solved jointly with the equation for the electron density: $\partial\rho/\partial\eta=W(\rho_0-\rho)+\sigma\rho I/U_i$. The ionization rate W is calculated using the Popov-Perelomov-Terentyev modification [27] of the Keldysh formula [28]. The impact ionization cross section σ is included in the model through the Drude formula $\sigma(\omega)=e^2\tau_c[m_e\varepsilon_0 n_0 c(1+\omega^2\tau_c^2)]^{-1}$, where τ_c is the electron collision time.

Our numerical algorithm is based on the split-step method, with a quasifast Hankel transform used to calculate the diffraction operator and the fifth-order Runge-Kutta method solving the equation for the electron density. An overall computational complexity of simulations is about 30 PFlop. The model was implemented in parallel codes, which were run on the Chebyshev and Lomonosov supercomputers at M.V. Lomonosov Moscow State University.

Our simulations were performed for typical conditions of filamentation experiments in a gas mixture consisting of 1 atm molecular nitrogen and 5 atm argon with the laser sources of ultrashort pulses at central wavelengths of 1.03 and 3.9 μm. To model these experiments, we set $n_{2,\mathrm{Ar}}=0.9\times10^{-19}\ (p/p_{\mathrm{atm}})\ \mathrm{cm}^2/\mathrm{W}$ for argon, $n_{2,\mathrm{N2}}=4.5\times10^{-19}(p/p_{\mathrm{atm}})\ \mathrm{cm}^2/\mathrm{W}$ for nitrogen [29,30], and $\rho_0=2.7\times10^{19}(p/p_{\mathrm{atm}})\ \mathrm{cm}^{-3}$, where p is the partial gas (argon or nitrogen) pressure and p_{atm} is the atmospheric pressure. The nonlinear coefficient n_4 is estimated as $n_4=-2\times10^{-33}\ \mathrm{cm}^4/\mathrm{W}^2$ [31] for the considered gas mixture. The Raman response function of molecular nitrogen was modeled using the damped oscillator approximation $R(\eta)=\sin(\eta/\tau_1)\exp(-\eta/\tau_2)$, with time constants τ_1 and τ_1 determined with the use of the method developed by Nibbering *et al.* [30] from the best fit of the spectral profile of the Raman response of molecular nitrogen, yielding $\tau_1=62.5$ fs and $\tau_2=120$ fs. The collision time constant in the Drude model is taken equal to 350 (p_{atm}/p) fs [7]. Gas dispersion was included in the model through the standard Sellmeier equation for the near-IR range [30] and through the Mathar model [32] with use of the HITRAN database [33] for the mid-IR range (see also Ref. [34]).

Results of numerical modeling of filamentation dynamics of laser pulses are presented in Fig. 7. In these simulations, the laser peak power P was kept close to the critical power of self-focusing P_{cr}. Under this condition our model was shown to provide good agreement with experimental results in mid-IR filamentation in argon [35]. As follows from Fig. 6, the mid-IR filament is longer, has larger diameter, and provides higher electronic density in comparison to the near-IR filament under the condition of fixed P/P_{cr} ratio. Results of these simulations were used as input parameters for the simulation of plasma dynamics and population kinetics in the wake of the mid-IR laser pulses.

B. Plasma kinetics modeling

We describe a change of concentration of different neutral and ionic atomic and molecular species in the filament plasma by the following set of rate equations:

$$\frac{d[N_s]}{dt}=[G_s]-[L_s], \quad (2)$$

where the subscript s stands for e, Ar^+, $Ar_2{}^+$, $N_2{}^+$, $N_4{}^+$, $N_3{}^+$, N^+, N, $N_2(A^3\Sigma_u)$, $N_2(B\,^3\Pi_g)$, $N_2(C\,^3\Pi_u)$, and $Ar^*(4\,^3P_2)$; N_s is the density of species of type s; and G_s and L_s are the relevant generation and loss rates. The detailed description of the model and the full list of included reactions can be found in Ref. [14]. In comparison with [14], the model was extended by including transitions from the $N_2(C\,^3\Pi_u)$ state to the first excited vibrational state of $N_2(B\,^3\Pi_g)$. Corresponding constants for processes of generation and loss of $N_2(B\,^3\Pi_g)_{v=0}$ and $N_2(B\,^3\Pi_g)_{v=1}$ are taken from [36].

The rate equations (2) are solved jointly with the equations for the electron temperature and the vibrational temperature of ground-state nitrogen molecules:

$$\frac{3}{2}k\frac{d}{dt}(N_eT_e)=-\frac{3}{2}N_ek(T_e-T_{\mathrm{vibr}})\nu_*$$
$$-\frac{3}{2}N_ek(T_e-T)\left[\delta_{N_2}\left(\nu_{N_2}+\nu_{N_2^+}+\frac{1}{2}\nu_{N_4^+}\right)\right.$$
$$\left.+\delta_{Ar}\left(\nu_{Ar}+\nu_{Ar^+}+\frac{1}{2}\nu_{Ar_2^+}\right)\right]$$
$$+k_eN_eN_{Ar^*}I_{\mathrm{exc}}, \quad (3)$$

$$\frac{dT_{\mathrm{vibr}}}{dt}=(N_e/N_{N_2})(T_e-T_{\mathrm{vibr}})\nu_*-(T_{\mathrm{vibr}}-T)$$
$$\times[1/\tau_{\mathrm{VT},N_2}+(N_{Ar}/N_2)/\tau_{\mathrm{VT,Ar}}], \quad (4)$$

where the first term in the right-hand part of Eq. (3) is related to the electron energy transfer to vibrational excitation of nitrogen molecules; the second term to the electron energy transfer in elastic and Coulombic collisions to translational energy of nitrogen and argon molecules, atoms, and ions; k is the Boltzmann constant; T, T_e, and T_{vibr} are the gas, electronic, and vibrational temperatures, respectively; ν_s are the frequencies

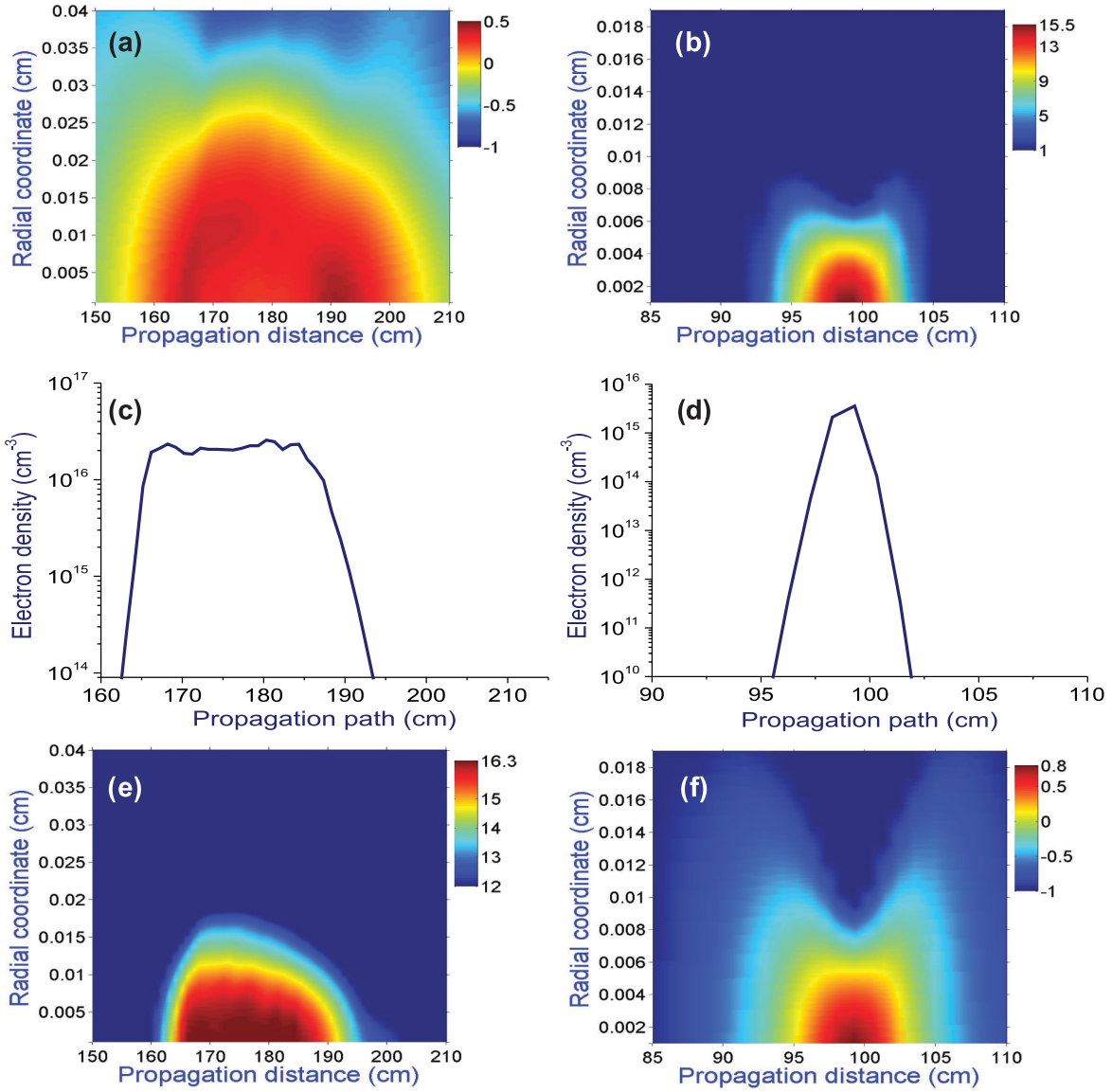

FIG. 7. (Color online) The on-axis electron density (in cm^{-3} on the logarithmic scale) calculated as a function of the propagation coordinate z and the radial coordinate r in the wake of the laser pulse (a, b), the longitudinal profiles of the on-axis electron density in the wake of the laser pulse (c, d), and the fluence (in arbitrary units on the logarithmic scale) calculated as a function of z and r (e, f) for laser pulses with a central wavelength $\lambda_0 = 3900$ nm, $W_0 = 7$ mJ, and $\tau_0 = 80$ fs (a,c,e) and $\lambda_0 = 1030$ nm, input pulse energy $W_0 = 0.4$ mJ, and initial pulse width $\tau_0 = 200$ fs (b, d, f) in a gas mixture consisting of 1 atm molecular nitrogen and 5 atm argon.

of elastic collisions of electrons and corresponding species; ν_* is the frequency of inelastic collisions of electrons with N_2 in the ground state which are responsible for vibrational heating; $\delta_{N_2} = 2m/M_{N_2}$, $\delta_{Ar} = 2m/M_{Ar}$; k_e is the deexcitation rate of excited argon atoms by electrons; $\tau_{VT,N2}$ and $\tau_{VT,Ar}$ are the vibrational relaxation times due to N_2-N_2 and N_2-Ar collisions, respectively, calculated using the Landau-Teller approximation (see Ref. [14]); and $I_{exc} \approx 11.8$ eV stands for the argon excitation energy into Ar*(4^3P_2). The initial energy of electrons in the wake of the mid-IR laser pulse was taken equal to 1 eV ($T_e = 0.66$ eV). The initial translational temperature of atoms and molecules in the gas mixture and the vibrational temperature of nitrogen molecules were set equal to $T = T_V = 290$ K.

To include the lasing effects, the set of plasma kinetic equations is completed by the relevant rate equations for the populations of the lasing levels and number of generated photons:

$$\begin{aligned}
\frac{dn_C}{dt} &= S_C - n_C(A_{CB1} + A_{CB2} + \sigma_{CB1}cn_{ph1} + \sigma_{CB2}cn_{ph2}) \\
&\quad + n_{B1}\sigma_{B1C}cn_{ph1} + n_{B2}\sigma_{B2C}cn_{ph2}, \\
\frac{dn_{B1}}{dt} &= S_{B1} + n_C(A_{CB1} + \sigma_{CB1}cn_{ph1}) - n_{B1}\sigma_{B1C}cn_{ph1}, \\
\frac{dn_{B2}}{dt} &= S_{B2} + n_C(A_{CB2} + \sigma_{CB2}cn_{ph2}) - n_{B2}\sigma_{B2C}cn_{ph2}, \\
\frac{dn_{ph1}}{dt} &= \frac{\sigma_{CB1}(n_C - n_{B1})n_{ph1}c}{1 + I_L/I_{s1}} - \frac{n_{ph1}}{\tau_{ph}}, \\
\frac{dn_{ph2}}{dt} &= \frac{\sigma_{CB2}(n_C - n_{B2})n_{ph2}c}{1 + I_L/I_{s2}} - \frac{n_{ph2}}{\tau_{ph}}.
\end{aligned} \tag{5}$$

Here n_C is the population of the $C\,^3\Pi_u$ state, $n_{B1,B2}$ are the populations of $B\,^3\Pi_g$ in the ground and first excited vibrational states, respectively; S are the rates of generation and loss through all the nonradiative channels; σ are the stimulated emission cross sections; c is the speed of light; $I_s = h\nu/\sigma(\upsilon)\tau_s$ are the saturation intensities where the radiative lifetimes $\tau_s \propto A^{-1}$ were determined from the corresponding Einstein coefficients; $I_l = n_{\rm ph} h\nu c$ are the lasing intensities; and $n_{\rm ph1,2}$ are the photon number densities at $\lambda = 337$ and 357 nm; $\tau_{\rm ph}$ is a photon lifetime related with the filament length L as $\tau_{\rm ph} = L/c$. The broadening of each of the laser modes was assumed equal to $\Delta\lambda = 0.1$ nm. The pressure-induced line broadening was taken as in Ref. [34], $g(\nu) \approx g_0(\nu)760/(p_{\rm Ar} + p_{\rm N_2})$, where $g_0(\nu)$ is the spectral line shape at the gas pressure $p = 760$ Torr and $T = 300$ K, and $p_{\rm Ar}$ and $p_{\rm N2}$ are the partial pressures of argon and molecular nitrogen.

The set of equations (2)–(5) is a so-called 0-dimensional time-dependent model which is one of the standard models for description of chemical and plasma-chemical kinetics. The variables in the model (2)–(5) are functions of time only, implying that we neglect spatial effects like diffusion and spatial gain inhomogeneity, and revealing the meaning of "0-dimensional" in the model's name.

The results of numerical solution for the system of equations (2)–(5), performed for the filament with an electron density of 10^{17} cm^{-3} in a gas mixture containing 1 bar N_2 and 5 bar Ar, are presented in Fig. 8. Population inversion builds up approximately 1 ns after the filament formation, with the maximum ratio of the $C\,^3\Pi_u$ and $B\,^3\Pi_g$ populations equal to 10:1. This ratio is very close to the maximum population inversion in an electron-impact-pumped nitrogen laser. Calculating the gain as $g = \sigma\Delta n$, where σ is an emission cross section obtained from the values of the Einstein constants given in Ref. [37], Δn is inversion population density, and comparing with the minimum value of gain enabling lasing given above, we can estimate from Fig. 7 that laser generation is possible within the time window of about 4 ns. This estimation is in reasonable agreement with the measured duration of the generated pulses. In spite of large simplicity

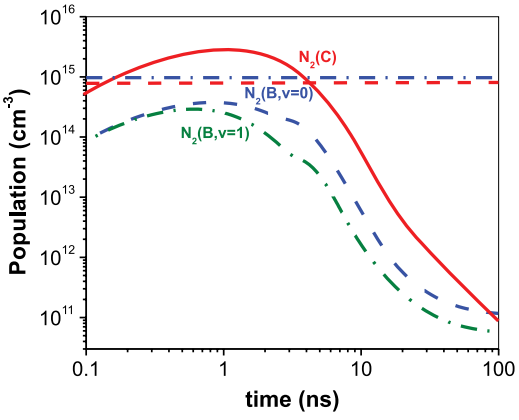

FIG. 8. (Color online) Population dynamics simulated using Eqs. (1)–(4) for the $C\,^3\Pi_u$ (red solid curve), $B\,^3\Pi_g$ (blue dashed curve), $B\,^3\Pi_g$ (green dot-dashed curve) of molecular nitrogen in the wake of the filament. Dashed and dash-dotted lines show minimum values of populations for $C\,^3\Pi_u$ state enabling lasing at 337 and 357 nm wavelengths, respectively.

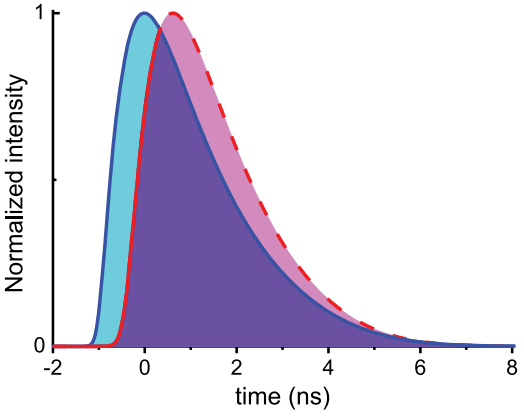

FIG. 9. (Color online) Numerically calculated pulses of the UV emission at 337 nm (blue solid line) and 357 nm (red dotted line).

of the model (2)–(5), our simulations accurately reproduce the experimental time delay between the 337– and 357–nm pulses, as it is shown in Fig. 9. An important insight provided by our model is that this delay occurs because the gain for the $\nu = 1 \rightarrow 0$ transition is lower than the gain for the $\nu = 0 \rightarrow 0$ transition, which leads to a slower buildup of lasing at 357 nm. Also, the calculated pressure dependencies of the stimulated emission yield are in good agreement with the measurements.

IV. CONCLUSION

In conclusion, we present a proof of the possibility for remotely initiated lasing from molecular gases by femtosecond filaments. We have demonstrated that a midinfrared femtosecond laser filament can induce backward-directed lasing of molecular nitrogen via a resonant excitation transfer mechanism. We performed full characterization of the filament-ignited nitrogen laser, including detailed investigations of spatial and temporal properties of the generated UV emission and generation thresholds. We have shown that a filament-assisted nitrogen laser can be at least as efficient as its conventional discharge-pumped counterpart. Mid-IR ultrashort laser pulses have been shown to radically enhance filamentation-assisted lasing of N_2 relative to ultrashort pulses in the near-IR. An accurate quantitative comparison between experimental results and simulations will only be possible with a full analysis of multiple filamentation. We believe that our results are a very important step on the route toward a remotely pumped N_2 laser in the atmosphere. Accomplishing this goal will require a deeper understanding and optimization of the pumping via electron-N_2 collisions and may involve the use of additional, long-pulse light, as it was suggested in Ref. [4], or microwave sources in combination with the femtosecond filament.

ACKNOWLEDGMENTS

This research was conducted as part of the EU FP7 Project CROSS TRAP (STREP 244068) funded by the European Commission. S.L.C. acknowledges the support of the Canada Research Chairs Program, NSERC, FQRNT, and CIPI. A.Z. acknowledges a valuable help from A. A. Voronin and a partial support of his research by the Welch Foundation (Grant No. A-1801) and the Russian Foundation for Basic Research.

[1] L. E. S. Mathias and J. T. Parker, Appl. Phys. Lett. **3**, 16 (1963).
[2] N. G. Heard, Nature (London) **200**, 667 (1963).
[3] http://www.crosstrap.eu
[4] P. R. Hemmer, R. B. Miles, P. Polynkin, T. Sieberta, A. V. Sokolov, P. Sprangle, and M. O. Scully, PNAS **108**, 3130 (2011).
[5] V. A. Vaulin, V. N. Slinko, and S. S. Sulakshin, Sov. J. Quantum Electron. **18**, 1457 (1988).
[6] A. Braun *et al*., Opt. Lett. **20**, 73 (1995).
[7] A. Couairon and A. Mysyrowicz, Phys. Rep. **441**, 47 (2007).
[8] L. Bergé, S. Skupin, R. Nuter, J. Kasparian, and J.-P. Wolf, Rep. Prog. Phys. **70**, 1633 (2007).
[9] J. Kasparian and J.-P. Wolf, Opt. Express **16**, 466 (2008).
[10] V. P. Kandidov, S. A. Shlenov, and O. G. Kosareva, Quantum Electron. **39**, 205 (2009).
[11] S. L. Chin, S. A. Hosseini, W. Liu, Q. Luo, F. Théberge, N. Aközbek, A. Becker, V. P. Kandidov, O. G. Kosareva, and H. Schroeder, Can. J. Phys. **83**, 863 (2005).
[12] S. L. Chin, *Femtosecond Laser Filamentation*, Springer Series on Atomic, Optical and Plasma Physics, Vol. 55 (Springer Science + Business Media, LLC, 2010).
[13] Y. P. Raizer, *Gas Discharge Physics* (Springer, New York, 1987).
[14] M. N. Shneider, A. Baltuška, and A. M. Zheltikov, J. Appl. Phys. **110**, 083112 (2011).
[15] A. Dogariu, J. B. Michael, M. O. Scully, and R. B. Miles, Science **331**, 442 (2011).
[16] Q. Luo, W. Liu, and S. L. Chin, Appl. Phys. B **76**, 337 (2003).
[17] R. S. Kunabenchi, M. R. Gorbal, and M. I. Savadatt, Prog. Quantum Electron. **9**, 259 (1984).
[18] C. P. Malone, P. V. Johnson, I. Kanik, B. Ajdari, and M. A. Khakoo, Phys. Rev. A **79**, 032704 (2009); C. P. Malone, P. V. Johnson, I. Kanik, B. Ajdari, S. S. Rahman, S. S. Bata, A. Emigh, and M. A. Khakoo, *ibid*. **79**, 032705 (2009).
[19] J. Kasparian, R. Sauerbrey, and S. L. Chin, Appl. Phys. B **71**, 877 (2000).
[20] A. Becker, N. Aközbek, K. Vijayalakshmi, E. Oral, C. M. Bowden, and S. L. Chin, Appl. Phys. B **73**, 287 (2001).
[21] W. R. Bennett, W. L. Faust, R. A. McFarlane, and C. K. N. Patel, Phys. Rev. Lett. **8**, 470 (1962); W. R. Bennett Jr., Ann. Phys. **18**, 367 (1962).
[22] G. Andriukaitis, T. Balčiūnas, S. Ališauskas, A. Pugžlys, A. Baltuška, T. Popmintchev, M.-C. Chen, M. M. Murnane, and H. C. Kapteyn, Opt. Lett. **36**, 2755 (2011).
[23] D. Kartashov, S. Ališauskas, A. Pugžlys, A. Voronin, A. Zheltikov, M. Petrarca, P. Béjot, J. Kasparian, J.-P. Wolf, and A. Baltuška, Opt. Lett. **37**, 3456 (2012).
[24] L. Pereira, A. Morozov, M. M. Fraga, T. Heindl, R. Krücken, J. Wieser, and A. Ulrich, Eur. Phys. J. D **56**, 325 (2010).
[25] A. Kossyi, A. Yu. Kostinsky, A. A. Matveyev, and V. P. Silakov, Plasma Sources Sci. Technol. **1**, 207 (1992).
[26] A. A. Voronin, S. Ališauskas, O. D. Mücke, A. Pugžlys, A. Baltuška, and A. M. Zheltikov, Phys. Rev. A **84**, 023832 (2011).
[27] A. M. Perelomov, V. S. Popov, and M. V. Terent'ev, Zh. Eksp. Teor. Fiz. **50**, 1393 (1966) [Sov. Phys. JETP **23**, 924 (1966)].
[28] L. V. Keldysh, Zh. Eksp. Teor. Fiz. **47**, 1945 (1964) [Sov. Phys. JETP **20**, 1307 (1965)].
[29] M. J. Weber, *Handbook of Optical Materials* (CRC Press, Boca Raton, FL, 2003).
[30] E. T. J. Nibbering,G. Grillon, M. A. Franco, B. S. Prade, and A. Mysyrowicz, J. Opt. Soc. Am. B **14**, 650 (1997).
[31] V. Loriot, E. Hertz, O. Faucher, and B. Lavorel, Opt. Express **17**, 13429 (2009).
[32] R. J. Mathar, Appl. Opt. **43**, 928 (2004).
[33] http://www.cfa.harvard.edu/hitran/
[34] D. Kartashov, S. Ališauskas, A. Pugžlys, A. A. Voronin, A. M. Zheltikov, and A. Baltuška, Opt. Lett. **37**, 2268 (2012).
[35] D. Kartashov, S. Ališauskas, A. Pugžlys, A. Voronin, A. Zheltikov, M. Petrarca, P. Béjot, J. Kasparian, J.-P. Wolf, and A. Baltuška, Opt. Lett. **37**, 3456 (2012).
[36] J. F. Loiseau, P. Plgnolet, and B. Held, J. Phys. D **25**, 745 (1992).
[37] C. O. Laux and C. H. Kruger, J. Quant. Spectrosc. Radiat. Transfer **48**, 9 (1992).